Control of meristem determinacy by trehalose-6-phosphate phosphatases is uncoupled from enzymatic activity

Hannes Claeys[1], Son Lang Vi[1,6], Xiaosa Xu[1], Namiko Satoh-Nagasawa[1,2,7], Andrea L. Eveland[3], Alexander Goldshmidt[1,8], Regina Feil[4], Grace A. Beggs[5], Hajime Sakai[2,9], Richard G. Brennan[5], John E. Lunn[4] and David Jackson[1]*

[1]Cold Spring Harbor Laboratory, Cold Spring Harbor, New York 11724, USA

[2]DuPont-Pioneer, Wilmington, Delaware 19803, USA

[3]Donald Danforth Plant Science Center, St Louis, Missouri 63132, USA

[4]Max Planck Institute of Molecular Plant Physiology, Potsdam, Germany

[5]Duke University, Durham, North Carolina 27710, USA

[6]Present address: Agricultural Genetics Institute, Hanoi, Vietnam

[7]Present address: Akita Prefectural University, Akita, Japan

[8]Present address: Institute of Plant Sciences, Agricultural Research Organization, Volcani Center, Bet Dagan, Israel

[9]Present address: Napigen, Wilmington, Delaware 19803, USA

*Corresponding author; http://orcid.org/0000-0002-4269-7649

Abstract

Meristem fate is regulated by trehalose-6-phosphate phosphatases (TPPs), but their mechanism of action remains mysterious. Loss of the maize TPPs *RAMOSA3* and *TPP4* leads to reduced meristem determinacy and more inflorescence branching. However, analysis of an allelic series revealed no correlation between enzymatic activity and branching, and a catalytically inactive version of RA3 complements the *ra3* mutant. Together with their nuclear localization, these findings suggest a moonlighting function for TPPs.

The body plan of plants is determined by meristems, self-renewing pools of pluripotent stem cells that produce new structures such as roots, leaves and floral organs. Meristem development is tightly controlled by multiple pathways[1], and an important regulator of meristem fate is the phosphorylated disaccharide trehalose 6-phosphate (T6P). For example, loss-of-function mutations in TREHALOSE-6-PHOSPHATE SYNTHASE1 (TPS1), the major enzyme for T6P biosynthesis in *Arabidopsis* (*Arabidopsis thaliana*), are embryo-lethal, and when rescued during embryogenesis, impair the transition to reproductive development[2]. In maize (*Zea mays*), *RAMOSA3* (*RA3*) encodes a TREHALOSE-6-PHOSPHATE PHOSPHATASE (TPP) that dephosphorylates T6P to trehalose[3]. *ra3* mutants have reduced meristem determinacy, leading to increased tassel branching and ectopic branching in ears[3]. Despite its central role in controlling growth and development, knowledge on how T6P functions is limited. T6P levels correlate with sucrose levels, and are thought to be a signal that maintains appropriate sucrose levels for the tissue and developmental stage[4]. However, the molecular targets of T6P remain largely elusive. Sucrose non-fermenting1-related kinase 1 (SnRK1) functions in T6P-mediated growth control[5], but the extent to which T6P signals through additional pathways is a subject of debate[4,6]. A better mechanistic understanding of T6P could increase crop yields, since expression of a rice TPP in developing maize ears enhances yields under drought[7], and treatment with plant-permeable analogues of T6P increases grain yield and drought tolerance in wheat[8].

To better understand how TPPs regulate meristem determinacy, we isolated genetic modifiers by mutagenizing *ra3* mutants using ethyl methanesulfonate (EMS) and screening for enhanced ear branching. In this screen, we identified four independent lines with mutations in the *RA3* paralog *TREHALOSE-6-PHOSPHATE PHOSPHATASE4* (*TPP4*, Zm00001d052227) that were

associated with increased ear branching (Fig. 1a,b). All four alleles had missense mutations in residues that were conserved among plant TPPs (Fig. 1c, Supplementary Fig. 1). We confirmed that *TPP4* was the causal gene by generating a null allele using CRISPR/Cas9, which enhanced *ra3* to the same extent as our EMS alleles (Supplementary Fig. 2). *tpp4* mutants had normal, unbranched ears in the presence of functional RA3, but increased ear and tassel branch number semidominantly in a *ra3* mutant background (Fig. 1a,b, Supplementary Fig. 3), and branches extended up the ear rather than being restricted to the base as in *ra3* single mutants (Fig. 1a). Therefore TPP4 is a fully redundant paralog of *RA3*, and accordingly its expression was lower than *RA3* in developing ears[9]. However, TPP4 was strongly upregulated in *ra3* mutants (Fig. 1d), suggesting it compensates for loss of *RA3* in a responsive backup circuit[10]. *In situ* hybridization with *TPP4*-specific probes showed that this compensation occurred specifically in the expression domain of *RA3*, which subtends spikelet pair meristems[3] (Fig. 1e). An additional TPP, TPP12, was also upregulated in developing *ra3* mutant ears (Fig. 1d, Supplementary Fig. 4), but CRISPR/Cas9-induced *tpp12* mutants did not enhance *ra3* ear branching (Supplementary Fig. 4), indicating that RA3 and TPP4 are the major TPPs affecting meristem determinacy.

To further investigate how TPPs affect inflorescence development, we measured T6P levels in developing ears of *ra3* and *ra3;tpp4-1* double mutants at the stage where *RA3* and *TPP4* expression peaks. Surprisingly, there was no difference in T6P levels compared to the B73 wild type (Fig. 2a). While it is possible that localized effects of loss of *RA3* and *TPP4* were masked by the analysis of entire ear primordia, we speculated that TPP4 enzymatic activity may not be important, consistent with the fact that our EMS-generated *tpp4* alleles did not affect motifs important for phosphatase activity. We modelled TPP4 structure using structures of similar TPPs,

and only the Ser167 residue mutated in tpp4-2 was close to the active site (Fig. 2b). We also predicted that mutating Ala325 to Thr in tpp4-1 would result in steric clash with the nearby highly conserved Phe302 residue and disrupt the catalytic pocket. However, residues mutated in tpp4-3 and tpp4-4 were far from the active site on exposed surface loops, where their effect on protein structure and activity was not obvious (Fig. 2b). To test our structural predictions, we asked if the proteins encoded by the different *tpp4* alleles could complement the *S. cerevisiae tpp* mutant Δ*tps2*[11]. Expression of wild-type *TPP4* rescued the *Δtps2* growth defect, while a negative control, $tpp4^{NYN}$, in which two catalytically important Asp residues were mutated to Asn, did not, suggesting enzymatic activity was required to complement the yeast mutant (Fig. 2c). We next tested our *tpp4* alleles, and while *tpp4-1* was unable to complement Δ*tps2*, partial complementation was observed for *tpp4-2*, *tpp4-3* and *tpp4-4*, suggesting that they maintain some level of activity, confirming our structural predictions (Fig. 2c). To validate these results and to measure enzymatic activity, we used purified MBP fusion proteins for *in vitro* assays. Similar to RA3[3], TPP4 activity was specific for T6P, and did not dephosphorylate other sugar phosphates (Supplementary Fig. 5). We quantified the degree of activity for different tpp4 alleles, and found that while tpp4-1 had no detectable activity, tpp4-2 had low activity, and tpp4-3 and tpp4-4 had significant activity, at ~25 and ~35% of wild-type levels, respectively (Fig. 2d).

We next used our *tpp4* allelic series to ask if the branching phenotype correlated with enzymatic activity. All alleles were backcrossed to *ra3* in B73 at least three times, and we phenotyped segregating populations grown in replicate in three different field locations. The degree of ear branching was normalized across locations using segregating controls to account for influence of environment on the phenotype. All *tpp4* alleles enhanced *ra3* semi-dominantly;

however, despite the differences in enzyme activity, all alleles affected ear branching to the same degree, resulting in a two-fold increase in *ra3*;*tpp4* heterozygotes (Pearson's r = -0.37, p = 0.17), and a five-fold increase in *ra3*;*tpp4* homozygotes (Pearson's r = -0.22, p = 0.43; Fig. 2e, Supplementary Fig. 6). These results strongly suggested that TPP enzymatic activity is not important for control of branching.

To further test this hypothesis, we engineered a version of RA3 with a single amino acid change ($RA3^{D110E}$) predicted to maintain overall protein structure while abolishing catalytic activity (Fig. 2f). Expression of this catalytically dead RA3 using its native promoter complemented the *ra3* phenotype, leading to a ~50% reduction in ear branch number compared to control siblings without the transgene (Fig. 2g). Similar partial complementation was seen in families expressing a wild-type version of RA3 from the same promoter (Fig. 2g), suggesting the partial complementation was due to insufficient promoter elements in our constructs. Complementation of *ra3* by a catalytically dead RA3 suggests that a non-enzymatic function is responsible for its role in meristem determinacy.

Regulatory functions were postulated for the TPP family in *Arabidopsis*, as its expansion is due to whole-genome duplications with a high degree of paralog retention, typical of regulatory proteins with stricter gene dosage requirements compared to enzymes[12]. A regulatory function was also proposed for rice TPP7, based on its low activity and lack of effect on T6P levels[13]. Some metabolic enzymes are known to have regulatory functions, a phenomenon known as moonlighting[14], and two other sugar metabolic enzymes, HEXOKINASE1 (HXK1) and the fructose-1,6-bisphosphatase FRUCTOSE INSENSITIVE1, exhibit moonlighting activity in Arabidopsis[15,16]. As HXK1 regulates transcription in the nucleus[15], we investigated the subcellular

localization of RA3 and TPP4. Both proteins were predominantly localized in the nucleus when transiently expressed in tobacco (Supplementary Fig. 7), and we confirmed this by immunolocalization using RA3-specific antibodies in developing maize ears (Fig. 3). Interestingly, RA3 localized to speckles in cytoplasmic and nuclear compartments (Fig. 3), and these are typically associated with regulation of RNA processing and transcription[17]. As TPPs lack DNA- or RNA-binding domains, it is likely their hypothetical nuclear role requires interaction with other proteins, consistent with our observation that mutations on the surface of TPP4 impair its role in meristem determinacy. While the exact mechanism remains to be resolved, exploiting the dual roles of TPPs may open avenues for further crop improvement. TPP4 itself maps to QTL and near genome-wide association SNPs for tassel branch number[18] and is in a region that shows strong evidence of selection during maize domestication and improvement[19], making it an especially attractive target for improvement of maize productivity.

Methods

Mapping

Pollen mutagenesis was performed as described[20] on *ra3-fea1* in B73 and *ra3-NI* in Mo17, and ~1500 M2 families were screened for enhanced branching. To generate F2 mapping populations, enhancer candidates were crossed to *ra3-fea1* in the W23 or B73 background, and the resulting F1s were selfed. For each mutant, two pools were created using DNA from about 30 F2 individuals with either enhanced or non-enhanced ear branching, and single nucleotide polymorphism (SNP) genotyping was performed using MaizeSNP50 BeadChip microarrays (Illumina). After removal of low-quality SNPs (GC > 0.6) and non-polymorphic SNPs (allele frequency < 0.2 or > 0.8 in both pools), smoothed allele frequencies and their ratios were calculated using R 3.1.0 to find peaks associated with enhanced branching. Pooled genomic DNA from enhanced M2 individuals was used to make a library for next-generation sequencing using the NEBNext Ultra DNA Library Prep Kit for Illumina (New England Biolabs), and the sample was sequenced on a single lane of Illumina HiSeq2500 to 10x coverage. Reads were mapped to the maize B73 reference genome (AGPv3, https://www.maizegdb.org/assembly) using bwa-mem[21], and SNPs called using the GATK unified genotyper[22]. High-confidence SNPs supported by at least three reads were selected if they were homozygous, and prioritized if they were G/C to A/T transitions and in exons within the mapping interval. To confirm the mutation and detect causal mutations in other alleles, TPP4 was amplified from genomic DNA of M2 populations of additional enhancer lines for Sanger sequencing.

Generation of CRISPR/Cas9-induced mutants

Guide RNAs (gRNAs) targeting *TPP4* and *TPP12* were designed using CRISPR-P[23] (http://cbi.hzau.edu.cn/crispr/), and an array containing four gRNAs expressed from independent maize U6-derived promoters[24] was synthesized, with gRNAs GCAGATTGCCAGCGCGTCCC and GTCGAGGTACCGCAGGGACA targeting *TPP4* and gRNAs GTAGTGTTCAAGCAAAGCCC and GTGATCTTGCTGGGAGTAAA targeting *TPP12*. This array was cloned into the pMCG1005-Cas9 binary vector and transformed into the Hi-II background[25]. Mutations were identified by Sanger sequencing, and mutants were backcrossed at least three times to *ra3-fea1*(B73) before phenotyping. The inserted T-DNA containing Cas9 and the gRNA array was eliminated after the first backcross to ensure stability of mutations.

Generation of transgenic complementation lines

To generate pRA3::RA3^{D110E} lines, the GAC codon coding for D110 was changed to GAG using site-directed mutagenesis of a *RA3* genomic construct that spanned from 3,311 bp upstream of the ATG to the end of the 3' UTR. To generate control pRA3::RA3-FLAG-HA lines, sequence encoding a FLAG tag followed by a triple HA tag was introduced just before the stop codon of *RA3* in the same genomic construct. The resulting constructs were cloned into the binary vector pAM1006 and transformed into Hi-II. Transgenic lines were backcrossed at least five times to *ra3-fea1*(B73) before phenotyping. Individuals carrying transgenes were identified by scoring resistance to the selectable marker and/or by PCR.

Phenotyping

For ear and tassel phenotyping, plants were grown in field locations in Cold Spring Harbor, NY or Lloyd Harbor, NY (June-September), or Valle De Banderas, Nayarit, Mexico (November-February). Ears and tassels were collected after anthesis to count branches. For scanning electron microscopy, developing ears were dissected around six weeks after planting, and mounted on stubs to image on a Hitachi S-3500N scanning electron microscope. All phenotyping experiments were performed on segregating populations, and each individual was genotyped.

Gene expression analysis

2-3 mm ears were dissected from 6-week old plants from a population segregating for *ra3* and *tpp4-1*, and immediately frozen in liquid nitrogen. Tissue was ground using tungsten beads in a mixer mill, and total RNA was extracted using the DirectZol RNA Miniprep Kit (Zymo Research) for ear tissue, according to the manufacturer's instructions. DNAse digestion and cDNA synthesis were performed using the iScript gDNA Clear cDNA Synthesis Kit (Bio-Rad). Quantitative real-time PCR was performed using Universal SybrGreen Master Mix (Bio-Rad) on the CFX96 Real-Time system (Bio-Rad). Primers GGTCCGTCCTGTTATTGATTG and ATTCCATCACCTCAGCTGGA were used for qRT-PCR detection of TPP12. *UBIQUITIN1 (UBQ1*, Zm00001d015327) was used for normalization (primers CCGCTTCAAGATGCAGATCTTTG and GAGACGGAGCACAAGGTGG).

RNA sequencing

Raw reads from previously described samples[9] were trimmed and filtered using Trimmomatic 0.36, and paired reads were aligned against maize AGPv4.39 using HiSat2 2.1.0[26]. Counts were generated using HTSeq 0.6.0[27] for all transcripts in the AGPv4.39 GTF, and differential expression

was assessed using edgeR 3.22.0[28] in R 3.5.0 after filtering for genes with cpm > 1 in N samples, where N represents the number of biological replicates. Members of the TPP family were identified using Gramene (http://www.gramene.org), and the two members that were not previously described[29] were named *TPP13* (Zm00001d006375) and *TPP14* (Zm00001d029371).

In situ hybridization

Developing ears (2-3 mm stage) were dissected from six-week old field-grown plants, followed by fixing, embedding and *in situ* hybridization as described[30], with 16h substrate incubation. *RA3* probes were as previously reported[3], and for *TPP4*, two fragments were amplified for each from cDNA using primer pairs GCCTACATGAGCGACGTGAT/CCTCTTCCTCAGCACCTTGA and GTTGGGACGATCGAGAAAGT/GGCGTAGTAGAGCTCCGACA, and subcloned into pCR2.1. Clones carrying inserts in both orientations were identified and sequence-verified to generate antisense or sense probes by *in vitro* transcription with T7 polymerase (Roche).

In vitro TPP activity assays

RA3, *TPP4* and *TPP12* coding sequences were cloned into pMAL-c5x (New England Biolabs), and site-directed mutagenesis was performed on pMAL-c5x-TPP4 to introduce the various point mutations described in the Results section. All sequences were verified by Sanger sequencing before transformation into the Rosetta *E. coli* strain. Cultures were grown to an OD_{600} of 0.6 at 37°C, cooled to 16°C prior to addition of isopropyl β-D-1-thiogalactopyranoside to a final concentration of 0.5 mM, and grown for an additional 12-16 hours at 16°C. Culture harvesting and purification of MBP-TPPs were performed with the pMAL expression system (New England

Biolabs) according to the manufacturer's instructions. Protein purity and concentration were assessed using SDS-PAGE gels. For *in vitro* assays, equal amounts of purified TPPs were incubated for 30 minutes at 28°C in buffer containing 10 mM Tris-HCl pH 7.6, 0.2 mM EDTA, 5 mM $MgCl_2$, 0.1 mg/mL BSA, and 0.5 mM T6P, S6P, G6P or F6P (Sigma-Aldrich). Phosphate release was measured using a colorimetric assay as OD_{600} using the Serine/Threonine Phosphatase Assay System (Promega). Activity was expressed as a percentage of the activity measured with purified recombinant TPP4.

Metabolite measurements

Developing ears (2-3 mm) were dissected from seven-week-old field-grown plants and immediately frozen in liquid nitrogen. T6P was extracted with chloroform-methanol and measured by high-performance anion-exchange chromatography coupled to tandem mass spectrometry[6].

Protein structure homology model

The Phyre2 web portal for protein modelling and prediction[31] was used to construct a homology model from the amino acid sequence of TPP4. The intensive search function of the web portal selected model templates 5GVX, 5DX9, 5DXF, 5HVO, 5LQD, and 3T5T, corresponding to *Mycobacterium tuberculosis* TPP[32], the *Cryptococcus neoformans* TPP(D24N)-T6P complex[33], the *Candida albicans* TPP N-terminal domain[33], the *Aspergillus fumigatus* TPS in complex with UDP and validoxylamine A[34], the *Streptomyces venezuelae* TPS[35], and a structurally similar transferase from *Streptomyces hygroscopus* (unpublished), respectively. The TPP structures were necessary

for modelling the phosphatase domain of TPP4, whereas the other structures including the TPS structures were incorporated for modelling the N-terminal domain of TPP4. From these templates, 96% of the residues were modeled at >90% confidence.

Yeast complementation

RA3 and *TPP4* coding sequences were cloned into pYX212[12], and site-directed mutagenesis was performed to introduce the various point mutations described in the Results section. All sequences were verified by Sanger sequencing before transformation into the *S. cerevisiae* YSH448 Δ*tps2* strain. Clones were grown in liquid culture in SD-Ura medium to an OD_{600} of 1, spotted on SD-Ura plates with and without 1M NaCl, and grown at either 30°C or 39°C for two days. Expression of TPP-HA fusion proteins was assessed by Western blot using monoclonal anti-HA antibody from mouse (Sigma-Aldrich, clone HA-7).

Tobacco infiltration

RA3 and TPP4 were cloned into pK7FWG2 and pK7WGF2[36], respectively, and transformed into *Agrobacterium tumefaciens* strain GV3101. Tobacco infiltrations were performed as described[37] with Agrobacterium at OD_{600} 0.05, and a strain expressing p19[38] was coinfiltrated with all constructs. After two days, leaves were stained with 1 μg/mL 4',6-diamidino-2-phenylindole (DAPI; Thermo Fisher Scientific), and GFP and DAPI fluorescence were imaged using a Zeiss LSM 710 confocal microscope. For Western blot, total protein was prepared from tobacco leaves[37], and GFP fusion proteins were detected using HRP-conjugated mouse anti-GFP antibody (Miltenyi Biotec).

1

2 ***Immunolocalization***

3 Antibodies against RA3 were generated in rabbits using a peptide consisting of the first 80
4 residues of RA3 fused to a His-tag (produced in *E. coli*) as the antigen, and purified using the same
5 peptide[39]. Immunolocalization was performed as described[39] on 2-3 mm ears harvested from six-
6 week old *ra3* and B73 plants. RA3 was detected using the purified primary antibody and Cy3-
7 coupled goat anti-rabbit IgG secondary antibody. Nuclei were counterstained with 3C5 mouse
8 monoclonal antibody[40,41] and Alexa Fluor 568-coupled anti-mouse secondary antibody. Imaging
9 was performed on a Zeiss LSM 710 confocal microscope.

10

11 ***Data availability***

12 The data that support the findings of this study are available from the corresponding author upon
13 request.

14

15 **Supplementary information**

16 Supplementary Figure 1. Positions of residues with EMS-induced tpp4 mutations in alignment of
17 TPPs from maize, Arabidopsis, *E. coli* and *S. cerevisiae*.

18 Supplementary Figure 2. A CRISPR/Cas9-induced *tpp4* mutant enhances *ra3*.

19 Supplementary Figure 3. *tpp4-1* enhances tassel branch number in a *ra3*-dependent manner.

20 Supplementary Figure 4. CRISPR/Cas9-induced *tpp12* mutant alleles do not enhance *ra3*.

21 Supplementary Figure 5. RA3 and TPP4 are active TPPs with high specificity for T6P.

22 Supplementary Figure 6. Ear and tassel branching in *ra3;tpp4* double mutants.

Supplementary Figure 7. RA3 and TPP4 are mostly nuclear when transiently expressed in tobacco leaves.

Acknowledgments

We thank Prof. Dr. Patrick Van Dijck for sharing the pYX212 vector, Dr. Krishnamurthy Rao for discussion of RA3 protein structure, Tim Mulligan for plant care, and Sylvain Pouzet, Gavriela Carver, and all other Jackson lab summer students for their enthusiastic involvement in some of this work. This work was supported by funding from the National Science Foundation (IOS-1238202 and IOS-1755141), a collaborative agreement with Dupont Pioneer, and the European Molecular Biology Organization (Long-Term Fellowship to H.C.). The metabolite analysis was supported by the Max Planck Society (R.F and J.E.L.).

Author contributions

H.C. performed all experimental procedures except for those listed below, prepared figures, and co-wrote the manuscript. A.G. and S.L.V. isolated and fine-mapped *tpp4-1*. A.L.E. analyzed *tpp4-1* whole-genome sequencing data. X.X. mapped *tpp4-3* and *tpp4-4*. N.S.N. performed immunolocalizations, under the supervision of H.S. R.F. performed metabolite measurements, under the supervision of J.E.L., who also co-wrote the manuscript. G.A.B. performed modelling of the TPP4 structure, supervised by R.G.B. D.J. supervised the research, assisted with mutant screening and co-wrote the manuscript.

1 **Figure legends**

2

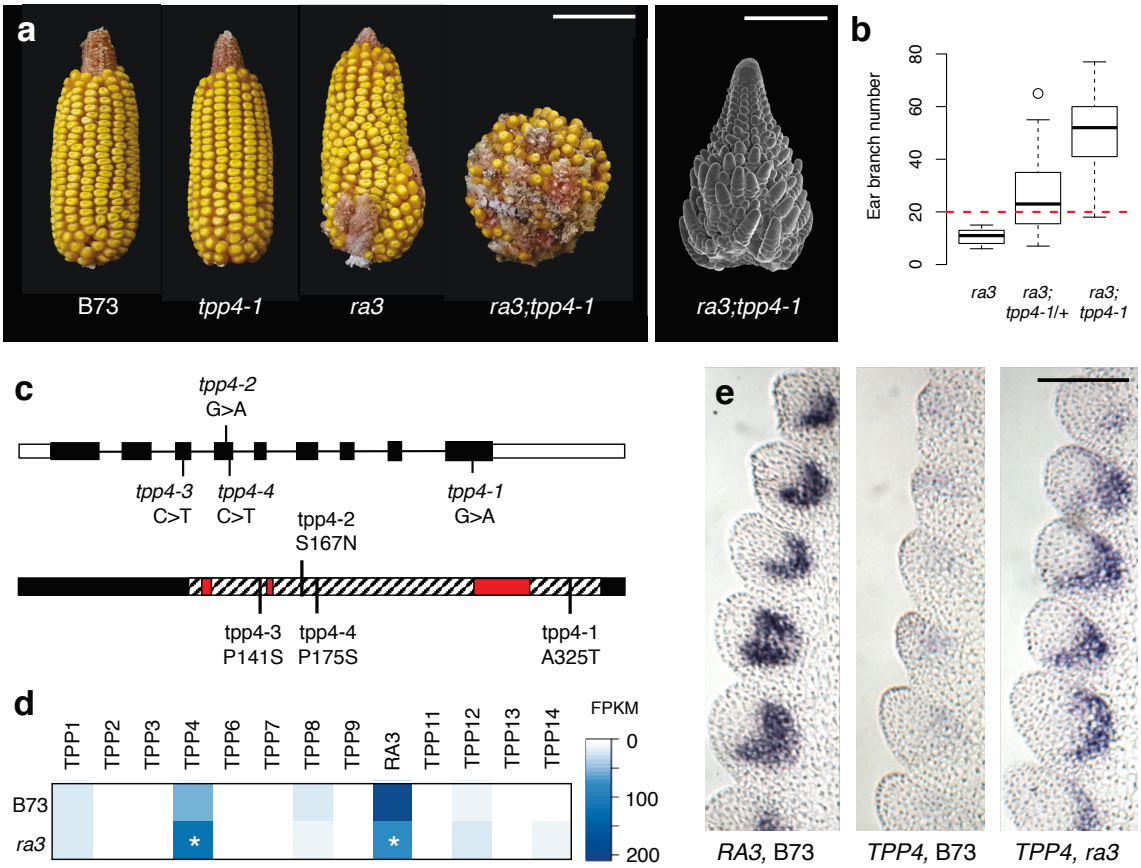

3

4 **Figure 1. TPP4 acts as a redundant back-up for RA3.**

5 **a**, Mature ears of B73 wild type, *tpp4-1*, *ra3* and *ra3;tpp4-1*, with enhanced branching compared

6 to *ra3*. Scale bar = 10 cm. An electron micrograph of a developing ra3;tpp4-1 ear on the right

7 shows branching extending up the ear. Scale bar = 1 mm. **b**, Co-segregation of *tpp4-1* with ear

8 branch number in a *ra3* mutant background. The red line indicates our arbitrary threshold for

9 enhancement (20 ear branches). N = 11;40;13. **c**, Overview of EMS-induced *tpp4* alleles. Top,

10 position of mutations in *TPP4*, with boxes indicating exons (CDS is in black) and lines indicating

11 introns. Bottom, positions of amino acid substitutions in the TPP4 protein, with the striped

12 portion indicating the TPP domain and conserved phosphatase boxes in red. **d,** Heatmap of

1 expression levels of all maize TPP genes in developing tassels and ears in wild type (B73) and *ra3*
2 mutants. TPP5 is a pseudogene and was excluded. Asterisks indicate differential expression
3 between B73 and *ra3* ears (FDR-adjusted $p < 0.05$, edgeR). **e,** *In situ* hybridization using an
4 antisense probe against *RA3* in a wild type B73 ear (left), showing expression subtending
5 developing spikelet pair meristems; and using an antisense probe against *TPP4* in a B73 (middle)
6 or a *ra3* mutant ear (right), showing TPP4 expression in the same domain, which is stronger in
7 *ra3* mutants. Scale bar = 100 µm.
8

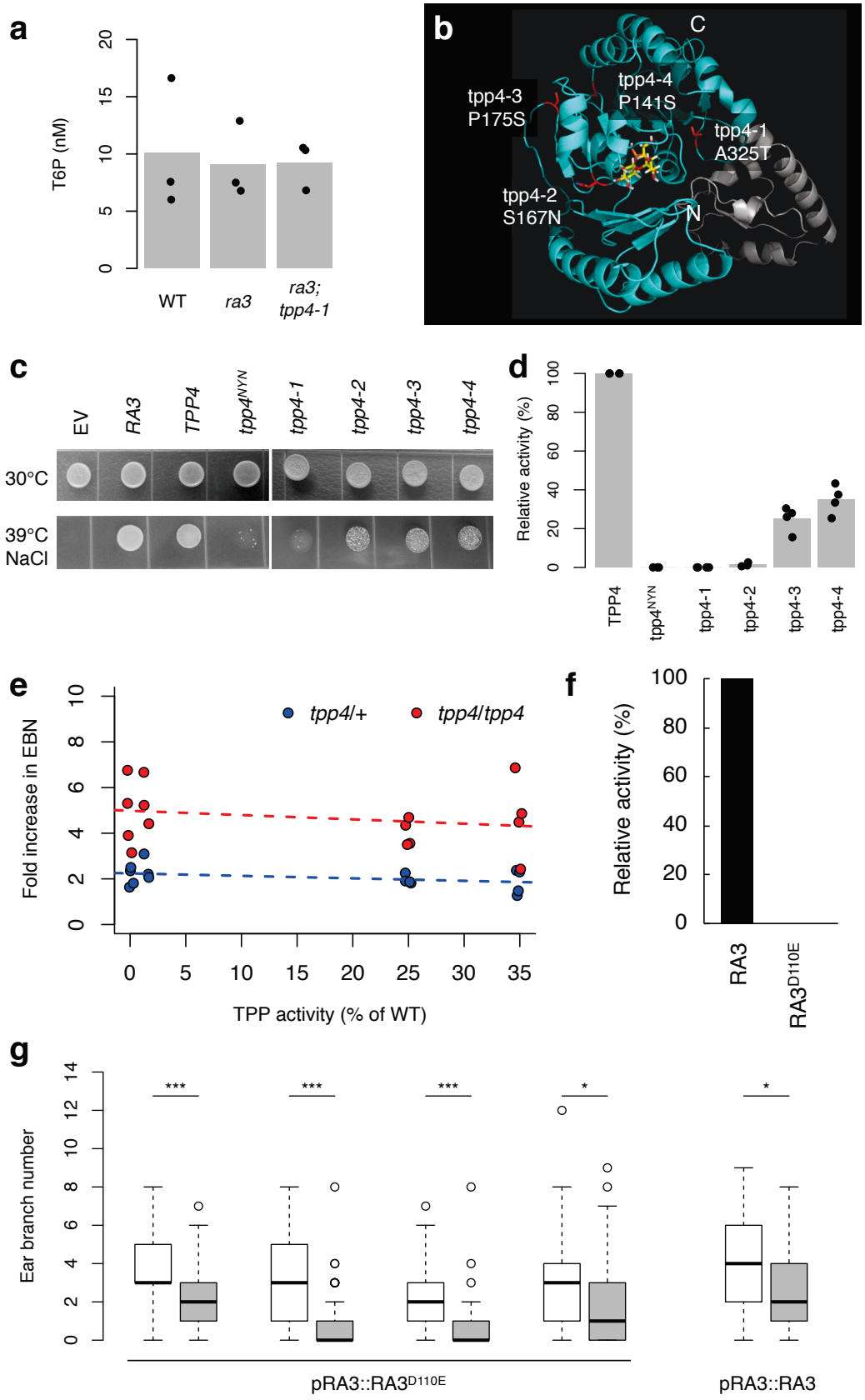
a
T6P (nM)
0
5
10
15
20
WT
ra3
ra3; tpp4-1
b
C
N
tpp4-3
P175S
tpp4-4
P141S
tpp4-1
A325T
tpp4-2
S167N
c
EV
RA3
TPP4
tpp4NYN
tpp4-1
tpp4-2
tpp4-3
tpp4-4
30°C
39°C
NaCl
d
Relative activity (%)
0
20
40
60
80
100
TPP4
tpp4NYN
tpp4-1
tpp4-2
tpp4-3
tpp4-4
e
Fold increase in EBN
0
2
4
6
8
10
tpp4/+
tpp4/tpp4
0
5
10
15
20
25
30
35
TPP activity (% of WT)
f
Relative activity (%)
0
20
40
60
80
100
RA3
RA3D110E
g
Ear branch number
0
2
4
6
8
10
12
14
***
***
***
*
*
pRA3::RA3D110E
pRA3::RA3

1

Figure 2. TPP enzymatic activity does not correlate with ear branching phenotype.

a, Levels of T6P are unchanged in extracts from immature ears of WT B73, *ra3* or *ra3;tpp4-1* mutants. Data points from three biological replicates are shown as dots; bars indicate the mean. **b,** Homology model of TPP4; the N-terminal extension is shown in grey and the TPP domain is in cyan; the N and C termini are labelled. Residues changed in the EMS mutants are shown in red, with all but Ser167 (*tpp4-2*) located on the protein surface. T6P is modeled in the active site in yellow. **c,** *RA3*, *TPP4*, and most *tpp4* EMS alleles complement the *Δtps2* yeast *tpp* mutant, whereas catalytically inactive $tpp4^{NYN}$ failed to complement. EV = empty vector (pYX212). **d,** tpp4-3 and -4 mutant proteins have considerable TPP activity. Dots indicate data points from four replicates; bars show the mean. **e,** Relative increase in ear branch number in *ra3;tpp4* heterozygote (blue) and *ra3;tpp4* homozygote (red) mutants compared to segregating single *ra3* mutants, plotted against TPP activity of the different alleles (from left to right, *tpp4-1*, *tpp4-2*, *tpp4-3* and *tpp4-4*). Note that there was no correlation between enzymatic activity and ear branching ($p = 0.17$ for heterozygous mutants, $p = 0.43$ for homozygous mutants). Dots indicate data points from four replicates, with trend lines shown as dotted lines. **f,** $RA3^{D110E}$ had no detectable TPP activity *in vitro*. **g**, Complementation of *ra3* by catalytically inactive $RA3^{D110E}$. Data are from segregating populations with siblings without the transgene in white and with the transgene in grey. Degree of complementation is similar for $RA3^{D110E}$ and wild-type RA3 constructs. *, $p < 0.05$; ***, $p < 0.001$; Student's t-test; N = 45;55; 39;53; 51;44; 43;43; 46;49.

1

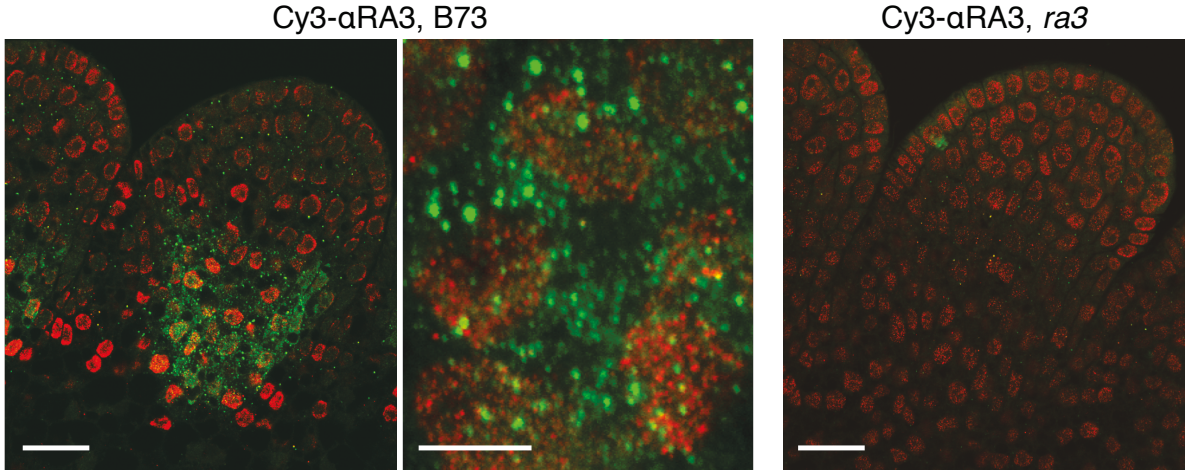

2

3 **Figure 3. RA3 localizes to nuclear and cytoplasmic speckles.**

4 Immunolocalization of native RA3 in nuclear and cytoplasmic speckles at the base of a spikelet

5 pair meristem, with RA3 in green and counterstained nuclei in red. Absence of signal in the *ra3*

6 mutant confirms the specificity of the antibody. Scale bar = 25 μm in the outer panels, 5 μm in

7 the middle panel.

8
9

References

1. Tanaka, W., Pautler, M., Jackson, D. & Hirano, H.-Y. Grass meristems II: inflorescence architecture, flower development and meristem fate. *Plant Cell Physiol.* **54,** 313–324 (2013).
2. van Dijken, A. J. H., Schluepmann, H. & Smeekens, S. C. M. Arabidopsis trehalose-6-phosphate synthase 1 is essential for normal vegetative growth and transition to flowering. *Plant Physiol.* **135,** 969–977 (2004).
3. Satoh-Nagasawa, N., Nagasawa, N., Malcomber, S., Sakai, H. & Jackson, D. A trehalose metabolic enzyme controls inflorescence architecture in maize. *Nature* **441,** 227–230 (2006).
4. Figueroa, C. M. & Lunn, J. E. A Tale of Two Sugars: Trehalose 6-Phosphate and Sucrose. *Plant Physiol.* **172,** 7–27 (2016).
5. Nunes, C. *et al.* The trehalose 6-phosphate/SnRK1 signaling pathway primes growth recovery following relief of sink limitation. *Plant Physiol.* **162,** 1720–1732 (2013).
6. Figueroa, C. M. *et al.* Trehalose 6-phosphate coordinates organic and amino acid metabolism with carbon availability. *Plant J.* **85,** 410–423 (2016).
7. Nuccio, M. L. *et al.* Expression of trehalose-6-phosphate phosphatase in maize ears improves yield in well-watered and drought conditions. *Nat. Biotechnol.* **33,** 862–869 (2015).
8. Griffiths, C. A. *et al.* Chemical intervention in plant sugar signalling increases yield and resilience. *Nature* **540,** 574–578 (2016).

9. Eveland, A. L. *et al.* Regulatory modules controlling maize inflorescence architecture. *Genome Res.* **24,** 431–443 (2014).
10. Kafri, R., Levy, M. & Pilpel, Y. The regulatory utilization of genetic redundancy through responsive backup circuits. *Proc Natl Acad Sci USA* **103,** 11653–11658 (2006).
11. De Virgilio, C. *et al.* Disruption of TPS2, the gene encoding the 100-kDa subunit of the trehalose-6-phosphate synthase/phosphatase complex in *Saccharomyces cerevisiae*, causes accumulation of trehalose-6-phosphate and loss of trehalose-6-phosphate phosphatase activity. *Eur. J. Biochem.* **212,** 315–323 (1993).
12. Vandesteene, L. *et al.* Expansive Evolution of the TREHALOSE-6-PHOSPHATE PHOSPHATASE Gene Family in Arabidopsis. *Plant Physiol.* **160,** 884–896 (2012).
13. Kretzschmar, T. *et al.* A trehalose-6-phosphate phosphatase enhances anaerobic germination tolerance in rice. *Nat Plants* **1,** 15124 (2015).
14. Copley, S. D. Moonlighting is mainstream: paradigm adjustment required. *Bioessays* **34,** 578–588 (2012).
15. Cho, Y.-H., Yoo, S.D. & Sheen, J. Regulatory Functions of Nuclear Hexokinase1 Complex in Glucose Signaling. *Cell* **127**, 579–589 (2006).
16. Cho, Y.-H. & Yoo, S.-D. Signaling role of fructose mediated by FINS1/FBP in Arabidopsis thaliana. *PLoS Genet.* **7,** e1001263 (2011).
17. Spector, D. L. & Lamond, A. I. Nuclear speckles. *Cold Spring Harb Perspect Biol* **3,** a000646 (2011).
18. Brown, P. J. *et al.* Distinct genetic architectures for male and female inflorescence traits of maize. *PLoS Genet.* **7,** e1002383 (2011).

19. Hufford, M. B. *et al.* Comparative population genomics of maize domestication and improvement. *Nat. Genet.* **44,** 808–811 (2012).

Supplemental references

20. Freeling, M. & Walbot, V. *The Maize Handbook*. (Springer-Verlag, 1994).
21. Li, H. Aligning sequence reads, clone sequences and assembly contigs with BWA-MEM. (2013).
22. McKenna, A. *et al.* The Genome Analysis Toolkit: A MapReduce framework for analyzing next-generation DNA sequencing data. *Genome Res.* **20,** 1297–1303 (2010).
23. Lei, Y. *et al.* CRISPR-P: A Web Tool for Synthetic Single-Guide RNA Design of CRISPR-System in Plants. *Mol Plant* **7,** 1494–1496 (2014).
24. Wu, Q., Regan, M., Furukawa, H. & Jackson, D. Role of heterotrimeric Ga proteins in maize development and enhancement of agronomic traits. *PLoS Genet.* **14,** (2018).
25. Char, S. N. *et al.* An Agrobacterium-delivered CRISPR/Cas9 system for high-frequency targeted mutagenesis in maize. *Plant Biotechnol. J.* **15,** 257–268 (2017).
26. Kim, D., Langmead, B. & Salzberg, S. L. HISAT: a fast spliced aligner with low memory requirements. *Nat. Methods* **12,** 357–360 (2015).
27. Anders, S., Pyl, P. T. & Huber, W. HTSeq--a Python framework to work with high-throughput sequencing data. *Bioinformatics* **31,** 166–169 (2015).
28. Robinson, M. D., McCarthy, D. J. & Smyth, G. K. edgeR: a Bioconductor package for differential expression analysis of digital gene expression data. *Bioinformatics* **26,** 139–140 (2010).

29. Zhou, M.-L. *et al.* Trehalose Metabolism-Related Genes in Maize. *J Plant Growth Regul* **33,** 256–271 (2014).

30. Jackson, D. P. in *Molecular Plant Pathology: A Practical Approach* (eds. Bowles, D. J., Gurr, S. J. & McPherson, M.) (1991).

31. Kelley, L. A., Mezulis, S., Yates, C. M., Wass, M. N. & Sternberg, M. J. E. The Phyre2 web portal for protein modeling, prediction and analysis. *Nat Protoc* **10,** 845–858 (2015).

32. Shan, S., Min, H., Liu, T., Jiang, D. & Rao, Z. Structural insight into dephosphorylation by trehalose 6-phosphate phosphatase (OtsB2) from *Mycobacterium tuberculosis*. *FASEB J.* **30,** 3989–3996 (2016).

33. Miao, Y. *et al.* Structures of trehalose-6-phosphate phosphatase from pathogenic fungi reveal the mechanisms of substrate recognition and catalysis. *Proc. Natl. Acad. Sci. U.S.A.* **113,** 7148–7153 (2016).

34. Miao, Y. *et al.* Structural and In Vivo Studies on Trehalose-6-Phosphate Synthase from Pathogenic Fungi Provide Insights into Its Catalytic Mechanism, Biological Necessity, and Potential for Novel Antifungal Drug Design. *mBio* **8,** e00643–17 (2017).

35. Asención Diez, M. D. *et al.* The Production and Utilization of GDP-glucose in the Biosynthesis of Trehalose 6-Phosphate by *Streptomyces venezuelae*. *J. Biol. Chem.* **292,** 945–954 (2017).

36. Karimi, M., Inzé, D. & Depicker, A. GATEWAY vectors for Agrobacterium-mediated plant transformation. *Trends Plant Sci.* **7,** 193–195 (2002).

37. Xu, F., Copeland, C. & Li, X. Protein Immunoprecipitation Using *Nicotiana benthamiana* Transient Expression System. *Bio-protocol* **5,** (2015).

38. Voinnet, O., Rivas, S., Mestre, P. & Baulcombe, D. An enhanced transient expression system in plants based on suppression of gene silencing by the p19 protein of tomato bushy stunt virus. *Plant J.* **33,** 949–956 (2003).

39. Smith, L. G., Greene, B., Veit, B. & Hake, S. A dominant mutation in the maize homeobox gene, *Knotted-1*, causes its ectopic expression in leaf cells with altered fates. *Development* **116,** 21–30 (1992).

40. Turner, B. M. & Franchi, L. Identification of protein antigens associated with the nuclear matrix and with clusters of interchromatin granules in both interphase and mitotic cells. *Journal of Cell Science* **87 (Pt 2),** 269–282 (1987).

41. Fang, Y., Hearn, S. & Spector, D. L. Tissue-specific expression and dynamic organization of SR splicing factors in Arabidopsis. *Mol. Biol. Cell* **15,** 2664–2673 (2004).